1-2003

Coherent Backscattering of Light in Atomic Systems: Application to Weak Localization in an Ensemble of Cold Alkali-Metal Atoms

D. V. Kupriyanov

I. M. Sokolov

P. Kulatunga
Old Dominion University

C. I. Sukenik
Old Dominion University, csukenik@odu.edu

M. D. Havey
Old Dominion University, mhavey@odu.edu

Coherent backscattering of light in atomic systems: Application to weak localization in an ensemble of cold alkali-metal atoms

D. V. Kupriyanov and I. M. Sokolov

Department of Theoretical Physics, State Technical University, 195251, St. Petersburg, Russia

P. Kulatunga, C. I. Sukenik, and M. D. Havey

Physics Department, Old Dominion University, Norfolk, Virginia 23529

Development of a theoretical treatment of multiple coherent light scattering in an ultracold atomic gas is reported. Specific application is made to coherent backscattering of a weak-radiation field from realistically modeled samples of ultracold atomic ^{85}Rb. Comprehensive Monte Carlo simulations of the spatial, spectral, and polarization dependence of the backscattering line shape are made and compared with available experimental results.

I. INTRODUCTION

Elastic and quasielastic scattering of light by elementary systems is a fundamental method of probing their internal or microscopic structure. The earliest exposition of this subject in modern form, focusing on light scattering from individual atoms, was made by Placzek [1] in 1934. Yet remarkable effects associated with the interaction of light and matter, including recent studies of ultraslow light propagation in atomic gases [2,3], macroscopically entangled quantum photonic states [4], and localization of light in complex media [5], continue to be dynamic areas of research in quantum optics. The quantitative aspects of the scattering typically depend on a characteristic length scale for the physical system in comparison to the wavelength of the light. For single-atom Rayleigh or Raman scattering, the scale of interest is of the order of the wavelength. However, for optically dense systems both coherent and incoherent multiple light scattering occurs; in this case the scattering mean free path and the physical size of the samples can also be important.

For near-resonant radiation propagating in optically dense media such as atomic or molecular gases, or for certain solid materials, multiple scattering can dominate the transmission and scattering properties of the medium. Although light propagation in this case is often thought to be diffusive, a wide range of remarkable phenomena associated with coherent radiative transport has been observed in solids and liquids [6,7]. First detailed observations of robust coherent effects in multiple light scattering were made of coherent backscattering, an effect in which light incident on a sample follows reciprocal paths through the material [8–10]. Identical phase accumulation for these paths results in constructive interference for light scattered into a narrow cone in the backward direction. The coherent backscattering effect and other multiple-scattering phenomena have found a wide range of applications to studies of light diffusion in biological samples, in acoustics, in characterization and calibration of nanoscale materials, and in planetary astronomy. A related important effect is lasing in random media [11,12], in which gain along reciprocal multiple-scattering paths can lead to mirrorless lasing in bulk material.

Coherent multiple light scattering is an observational indicator of weak localization of light [13,14], in which diffusion is inhibited by interference of reciprocal scattering paths in a material. When the scattering is strong enough diffusion may cease, and the light can become strongly localized. Such strong localization is a type of phase transition, in which ideally there exist localized states of light within a medium. Localization of this type is analogous to Anderson localization of electrons [15,16,6]. There has been to date two reports of such effects, one in the optical regime, and a second in the microwave region of the electromagnetic spectrum [5]. In that research, unique characteristics of both coherently backscattered light and the behavior of the intensity of the transmitted incoherent flux served as indicators of localization. In addition to these characteristics, it has recently been shown that there are strong statistical signatures of photon localization in random media [17,18].

Atomic gases form unique, especially well controlled and characterized systems in which to study light localization. Part of this is due to the very narrow width of atomic optical resonances, and that the multipolar atomic state distributions may be readily manipulated with external static or dynamic fields. In addition, the well-developed techniques of atom cooling and trapping [19] allow further control over the sample properties. Excitation of the atoms in the vicinity of resonances, and varying the polarization of the exciting light, permits variation of the scattering length and the tensor character of the localization effects [6,7]. The scattering from individual atoms, and the combined coherent effects of multiple Rayleigh and Raman scattering may also readily be modeled, at least in a far-field limit for the scattering. In gaseous atomic systems, however, coherent backscattering has only recently been observed in ultracold atomic samples confined in a magneto-optical trap [20–22]. These experiments have revealed a range of, as yet not completely understood, phenomena associated with sample density, detuning from resonance, sample size, and polarization [23,24]. In addition, recent experiments have shown strong magnetic-field-dependent spatial variations in the coherently backscattered intensity, both in atomic gases [22] and in turbid media [25]. Finally, even though it should be possible to observe coher-

ent backscattering from a thermal atomic vapor, to our knowledge no such experiments have yet been reported.

A main motivation of the research presented here is to theoretically examine the effects of weak localization of light in ultracold monoatomic gases. Of particular interest is the character of the coherent backscattering cone under conditions closely matched to those obtainable in experiments. These conditions include the size and optical depth of a sample of atoms confined in a magneto-optic trap. Also included is the important influence of radiative transitions among the hyperfine components of the atom, including elastic Rayleigh and Raman, and inelastic Raman transitions. We specifically report the spatial and spectral distribution and relative intensity of light scattered in the nearly backward direction for Rayleigh and Raman transitions in ^{85}Rb. A second focus of this paper is to illustrate the development of the theory of multiple coherent light scattering in atomic systems and in the weak-localization regime, with particular attention to the development of higher orders of light scattering. In this, we will be interested ultimately in the regime of strong localization of light, where the light may be trapped by multiple coherent scattering inside the atomic medium.

In the following sections, we first develop the theory used to describe multiple light scattering, starting with a review of the relevant aspects of single scattering of light from an atom in a weak field. This is followed by consideration of double scattering, and then generalizing to the case of multiple light scattering. Specific consideration is made of the effects of interference in multiple scattering and the transformation of the polarization of the incident beam into the near-backward direction. Consideration is then made of the details of the numerical simulation as applied to the coherent backscattering geometry. Results are presented and described for the spatial and polarization transformation of the incident light beam, in the multiply scattered regime, into the near-backscattering direction. Finally, the results are discussed in the context of recent experiments.

II. GENERAL THEORY

Consider a system of N identical atoms located in a finite volume and scattering coherent light of frequency ω. The wave of light incident on the atomic ensemble is assumed to be weak enough that possible saturation effects in its interaction with the atoms are negligible. The atomic ensemble, in general, represents an optically dense medium for resonance scattering, but, on the average, the atoms are separated by distances much larger than the wavelength $\lambdabar$. Thus each atom is located, on the average, in the radiation zone of its neighbors. The interaction of the atoms with incident and multiply scattered light is assumed to be of the dipole type and, as we will show, for a proper description of multiple scattering has to be restricted to the rotating wave approximation. In our analysis, we will ignore any possible effects due to dependent scattering, where light is scattered from pairs of interacting atoms; dependent scattering may be important for atom-atom separations less than a wavelength of light. As discussed in a recent review [26], and particularly in the context of radiative transport as shown in Ref. [27],

dependent scattering becomes important for a quite physically dense medium where the number of atoms per cubic wavelength becomes order of unity. In the present study, we are restricted to average densities an order of magnitude less than this, and so we ignore effects associated with nonradiative excitation transfer caused by long-range dipole-dipole interactions.

To follow as clearly as possible some analogy between classical and quantum descriptions of the coherent backscattering it seems convenient to solve the quantum problem in the Heisenberg picture. In such an approach, the basic process is the transformation of the electric-field operators in a single-scattering event. This process will be discussed at first, as an example of the transformation of the operator of the free electric field of a moving atom. As we establish, the field transformation in the single-scattering process is unitary and conserves the commutation relations. This allows us to make a subsequent generalization to the situation of an arbitrary number of scatterers. Then, we discuss the phenomenon of weak localization in an atomic ensemble containing a macroscopic number of atoms.

A. Transformation of the electric field in single scattering

The unperturbed electric-field operator in the origin of the coordinate frame coupled with a scattering atom, which moves with velocity $\mathbf{v}$, is given by

$$
\begin{aligned}
\hat{\mathbf{E}}_0(t) = \sum_{\mathbf{k}\mu} \left(\frac{2\pi\hbar\omega_k}{\mathcal{V}} \right)^{1/2} (-i) &[\mathbf{e}^*_{\mathbf{k}\mu} a^\dagger_{\mathbf{k}\mu} e^{i(\omega_k - \mathbf{k}\cdot\mathbf{v})t} \\
&- \mathbf{e}_{\mathbf{k}\mu} a_{\mathbf{k}\mu} e^{-i(\omega_k - \mathbf{k}\cdot\mathbf{v})t}] = \hat{\mathbf{E}}_0^{(-)}(t) + \hat{\mathbf{E}}_0^{(+)}(t), \quad (1)
\end{aligned}
$$

where $a^\dagger_{\mathbf{k}\mu}$, $a_{\mathbf{k}\mu}$ are, respectively, the operators of creation and annihilation of the photon with wave vector $\mathbf{k}$ and in the polarization state $\mathbf{e}_{\mathbf{k}\mu}$. $\mathcal{V}$ is the quantization volume. The second line in Eq. (1) defines negative and positive frequency components of the electric field.

The dipole-type interaction operator of the atom with the electric field is given by

$$
\hat{V}(t) = -\hat{\mathbf{d}}(t)\hat{\mathbf{E}}_0(t), \quad (2)
$$

where the operator for the atomic dipole moment $\hat{\mathbf{d}}(t)$ and for the electric field are defined in the interaction representation. Based on a perturbation theoretic approach, the exact solution for the Heisenberg operator can be written as the following expansion

$$
\hat{\mathbf{E}}(t) = \hat{\mathbf{E}}_0(t) + \hat{\mathbf{E}}_1(t) + \hat{\mathbf{E}}_2(t) + \cdots, \quad (3)
$$

which can be also written for positive $\hat{\mathbf{E}}^{(+)}(t)$ and negative $\hat{\mathbf{E}}^{(-)}(t)$ frequency components. We assume that the wave function of the joint atom-field system describes the combined state, where an atom occupies the ground state and the electric field is in the single-photon state or in a weak coherent state. Then the correction of the first order in Eq. (3) will disappear after averaging over the wave function. Thus, the second-order correction gives us the main contribution, since

it is responsible for the scattering process. The second-order term in Eq. (3) can be written as follows:

$$\hat{\mathbf{E}}_2(t) = -\frac{1}{\hbar^2} \int_0^t dt'' \int_{t''}^t dt'$$

$$\times [\hat{\mathbf{d}}(t'')\hat{\mathbf{E}}_0(t''), [\hat{\mathbf{d}}(t')\hat{\mathbf{E}}_0(t'), \hat{\mathbf{E}}_0(t)]]. \quad (4)$$

As follows from this expression, in a complete dynamical description of the process there is a memory of initial conditions in the formal expansion of perturbation theory. However, for nonsaturating fields this solution can be spread out over the time $t \gg \gamma^{-1}$, where γ is the natural radiative relaxation rate of the upper state. But in this case, it is necessary to take into account all the radiative corrections for retardation and the advanced Green's functions of the decaying upper atomic state. This can be done by introducing a natural decay law into the time behavior of the functions. Then the integral (4) loses its dependence on the lower limit, i.e., on the initial time coordinate.

The integral (4) gives us the solution for the electric field in the origin of the frame coupled with a moving atom. But in the zero order of relativistic effects, when only retardation effects in the radiation zone have to be taken into consideration, this solution coincides with the electric field in the laboratory frame at the point of atom location as well as in the small vicinity of this point. Then, we can obtain the solution for any point in the laboratory frame by using the propagation law in free space. By this procedure one obtains the following expansion for the positive frequency component of the electric-field operator in the radiation zone ($r \gg \lambda$) of the scattering atom,

$$\hat{\mathbf{E}}^{(+)}(\mathbf{r},t) = \hat{\mathbf{E}}_0^{(+)}(\mathbf{r},t) + \hat{\mathbf{E}}_2^{(+)}(\mathbf{r},t) + \cdots, \quad (5)$$

where

$$\hat{\mathbf{E}}_0^{(+)}(\mathbf{r},t) = \sum_{\mathbf{k}\mu} \left(\frac{2\pi\hbar\omega_k}{\mathcal{V}}\right)^{1/2} e^{-i(\omega_k t - \mathbf{k}\cdot\mathbf{r})} i\mathbf{e}_{\mathbf{k}\mu} a_{\mathbf{k}\mu}$$

and

$$\hat{\mathbf{E}}_2^{(+)}(\mathbf{r},t) = \sum_{m,m'} \sum_n \sum_{\mathbf{k}\mu} \left(\frac{2\pi\hbar\omega_k}{\mathcal{V}}\right)^{1/2} \frac{1}{ir} e^{-i\omega' t + ik' r}$$

$$\times |m'\rangle\langle m| a_{\mathbf{k}\mu} \frac{\omega'^2}{\hbar c^2} \left[-\frac{i(\mathbf{d}_\perp)_{nm}(\mathbf{d}\cdot\mathbf{e}_{\mathbf{k}\mu})_{m'n}}{i(\omega' + \omega_{nm} - \mathbf{k}'\cdot\mathbf{v})} \right.$$

$$\left. + \frac{i(\mathbf{d}_\perp)_{m'n}(\mathbf{d}\cdot\mathbf{e}_{\mathbf{k}\mu})_{nm}}{i(\omega_k - \omega_{nm} - \mathbf{k}\cdot\mathbf{v}) - \gamma_n/2} \right], \quad (6)$$

and the negative frequency component is given by the Hermitian conjugate, $\mathbf{E}^{(-)}(\mathbf{r},t) = \mathbf{E}^{(+)\dagger}(\mathbf{r},t)$. Here, the origin of the frame is chosen in the location of the atom, which is assumed to be unchanged during the light propagation time r/c. The scattered light frequency ω' is defined here via the

input frequency ω_k, and the Raman shift $\omega_{m'm}$ for atomic transition $|m\rangle \rightarrow |m'\rangle$. There is an additional Doppler shift caused by atomic motion, given by

$$\omega' \equiv \omega_{k'} = \omega_k - \omega_{m'm} + (\mathbf{k}' - \mathbf{k})\mathbf{v}. \quad (7)$$

The wave vector $\mathbf{k}' = \omega' \mathbf{r}/cr$, but in the right-hand side of Eq. (7) the Doppler correction is neglected and it is assumed that $\mathbf{k}' \approx \omega \mathbf{r}/cr$. The transition dipole moments in Eq. (6) are defined in the Schrödinger representation and its transverse component is given by

$$\hat{\mathbf{d}}_\perp = \hat{\mathbf{d}} - (\hat{\mathbf{d}} \cdot \mathbf{k}') \frac{\mathbf{k}'}{k'^2}. \quad (8)$$

The sum over n is expanded over all possible excited transitions characterized by natural linewidths γ_n, but as a practical matter, the sum can be restricted to the most significant resonance transitions and the frequency $\omega_k \equiv \omega$ can be associated with the frequency of the incident mode.

Based on Eq. (6), we can define the cross section of the Rayleigh-Raman single scattering of the photon $\omega, \mathbf{k}, \mathbf{e}$ into the mode $\omega', \mathbf{k}', \mathbf{e}'$ accompanied by the atomic transition $|m\rangle \rightarrow |m'\rangle$ as

$$d\sigma = \frac{\mathcal{V}}{2\pi\hbar\omega'} \langle [\mathbf{e}'^* \hat{\mathbf{E}}_2^{(+)}(\mathbf{r},t)]^\dagger \mathbf{e}'^* \hat{\mathbf{E}}_2^{(+)}(\mathbf{r},t)\rangle r^2 d\Omega'$$

$$= \frac{\omega\omega'^3}{\hbar^2 c^4} \left| \sum_n \left[-\frac{(\mathbf{d}\cdot\mathbf{e}'^*)_{nm}(\mathbf{d}\cdot\mathbf{e})_{m'n}}{i(\omega' + \omega_{nm} - \mathbf{k}'\cdot\mathbf{v})} \right. \right.$$

$$\left. \left. + \frac{(\mathbf{d}\cdot\mathbf{e}'^*)_{m'n}(\mathbf{d}\cdot\mathbf{e})_{nm}}{i(\omega - \omega_{nm} - \mathbf{k}\cdot\mathbf{v}) - \gamma_n/2} \right] \right|^2 d\Omega', \quad (9)$$

which coincides with the well-known Kramers-Heisenberg formula, [28]. The scattered radiation frequency ω' is expressed here in terms of the incident frequency ω via relationship (7) that takes into account possible frequency shifts caused by atomic motion.

The advantage of the Heisenberg approach is in the clear connection to a classical description. If in the brackets of Eq. (6), we leave only the major resonance term, and identify the electric-field operators as c numbers, then expansion of Eq. (5) will be quite similar to the corresponding classical expansion, where the atom can be treated as a model harmonic oscillator. One obtains in that case a complete coincidence with a classical model for a $^1S \rightarrow {}^1P$ resonance atomic transition.

B. Unitarity of the transformation

In spite of the fact that in Eq. (5), we keep only the leading nonvanishing terms of a full expansion, these terms still maintain the commutation relation for the electric-field operators, i.e., they reveal the unitary transformation of the field by a scatterer. Let us show here that

$$[\hat{E}_i^{(+)}(\mathbf{r},t),\hat{E}_j^{(-)}(\mathbf{r}',t)]=[\hat{E}_{0i}^{(+)}(\mathbf{r},t),\hat{E}_{0j}^{(-)}(\mathbf{r}',t)], \quad (10)$$

where the left-hand side is given by Eqs. (5) and (6). This result can be established with the following assumptions. First, we assume the spatial arguments to be located in the radiation zone of the scattering atom $r \gg \lambda$, which lets us expand the spherical wave in Eq. (6) in a set of plane waves in the small volume in the vicinity of some average point $\overline{\mathbf{r}}$ with the local direction of a z axis along $\overline{\mathbf{r}}$. Second, we leave only the quasiresonance term in Eq. (6) and restrict by this our proof to the rotating wave approximation. We additionally discuss below the importance of this approximation for fulfillment of Eq. (10).

As can be shown by straightforward calculation with these assumptions, one has

$$[\hat{E}_{2i}^{(+)}(\mathbf{r},t),\hat{E}_{0j}^{(-)}(\mathbf{r}',t)]+[\hat{E}_{0i}^{(+)}(\mathbf{r},t),\hat{E}_{2j}^{(-)}(\mathbf{r}',t)]$$

$$=-\frac{1}{3}\delta_{ij}\frac{1}{r^2}\int\frac{d\omega}{2\pi}e^{i\mathbf{k}(\mathbf{r}-\mathbf{r}')}\sum_{m,n}|m\rangle\langle m|\left(\frac{\omega}{c}\right)^4$$

$$\times\frac{|\mathbf{d}_{nm}|^2\gamma_n}{(\omega-\omega_{nm}-\mathbf{k}\cdot\mathbf{v})^2+\gamma_n^2/4}, \quad (11)$$

if $i,j=x$ or y and to be equal to zero, otherwise. The wave vector $\mathbf{k}$ under the spectral integral is given by $\mathbf{k}=\omega\overline{\mathbf{r}}/c\overline{r}$. On the other hand,

$$[\hat{E}_{2i}^{(+)}(\mathbf{r},t),\hat{E}_{2j}^{(-)}(\mathbf{r}',t)]$$

$$=+\frac{1}{3}\delta_{ij}\frac{1}{r^2}\int\frac{d\omega}{2\pi}e^{i\mathbf{k}(\mathbf{r}-\mathbf{r}')}\sum_{m,n}|m\rangle\langle m|\frac{\omega^3}{\omega_{nm}^3}\left(\frac{\omega}{c}\right)^4$$

$$\times\frac{|\mathbf{d}_{nm}|^2\gamma_n}{(\omega-\omega_{nm}-\mathbf{k}\cdot\mathbf{v})^2+\gamma_n^2/4}, \quad (12)$$

if $i,j=x$ or y and is equal to zero otherwise. Here, we neglected the difference between ω and ω' in the slowly varying functions in the vicinity of resonance $\omega\sim\omega_{nm}$.

The integrals on the right-hand sides of Eqs. (11) and (12) are nonconverging. This indicates the insufficiency of a dipole-type approximation for high frequencies. But both the expressions are actually valid in the assumption that the spectral band, contributed in the spectral integrals, is in the region surrounding the resonance transition $\omega\sim\omega_{nm}$. That is, the basic idea of the rotating wave approximation. In this case, the right-hand sides of Eqs. (11) and (12) are equal in magnitude but have opposite signs. So, we see that these terms compensate one another and, thus, the transformation of Eqs. (5) and (6) does not violate the commutation relation, i.e., they reveal the unitary transformation.

As a consequence of this there is no modification of any Green's propagation function of the field perturbed by the atom in a vicinity of any spatial point in its radiation zone, where another atom can be located. Thus, the fourth-order

term in correction of the electric-field perturbed by two atoms can be calculated via evaluation of the integral (4) near the location of the second atom, by substituting there the modified electric-field operators (5) and (6). While evaluating this integral, we can use the Green's function of a free field. In turn, this lets us make the next-step correction for the double-scattering case by double action of the transformation (5) and (6). It should be kept in mind always, that, in this procedure, we are strongly restricted in the approach by the rotating wave approximation.

C. Double scattering

Consider the double scattering of the photon $\omega,\mathbf{k},\mathbf{e}$ sequentially by atom 1, located at the point $\mathbf{r}_1$ and then by atom 2, located at the point $\mathbf{r}_2$. In the output channel, we detect the photon $\omega',\mathbf{k}',\mathbf{e}'$. In the backscattering limit the propagation direction of the output photon $\mathbf{k}'$ is assumed to be close to the direction $-\mathbf{k}$.

It is convenient to describe the fourth-order correction of the field operator in terms of a scattering tensor, see Ref. [28]. Let us define the scattering tensor in operator form as

$$\hat{\alpha}_{ji}^{(m'm)}(\omega)=-\sum_n|m'\rangle\langle m|\frac{(d_j)_{m'n}(d_i)_{nm}}{\hbar(\omega-\omega_{nm})+i\hbar\gamma_n/2}$$

$$\equiv|m'\rangle\langle m|\alpha_{ji}^{(m'm)}(\omega), \quad (13)$$

which is responsible for the Rayleigh-Raman scattering associated with an atomic transition $|m\rangle\rightarrow|m'\rangle$. According to the above discussion, we keep here only the leading quasiresonant contribution.

Then, the fourth-order correction to the positive frequency component of the electric-field amplitude for successive scattering on atom 1 and 2 is given by

$$\hat{\mathbf{E}}_{4;1\rightarrow2}^{(+)}(\mathbf{r},t)=\frac{1}{|\mathbf{r}-\mathbf{r}_2|r_{12}}$$

$$\times\sum_{m_1,m_1'}\sum_{m_2,m_2'}\sum_\nu\sum_{ij}\sum_{\mathbf{k},\mu}\left(\frac{2\pi\hbar\omega_k}{\mathcal{V}}\right)^{1/2}$$

$$\times\frac{\omega_2^2}{c^2}\frac{\omega_{12}^2}{c^2}\exp(-i\omega_2 t+ik_2|\mathbf{r}-\mathbf{r}_2|$$

$$+ik_{12}r_{12}+i\mathbf{k}\cdot\mathbf{r}_1)\mathbf{e}_{\mathbf{k}'\nu}\hat{\alpha}_{\nu i}^{(m_2'm_2)}(\omega_{12}-\mathbf{k}_{12}\mathbf{v}_2)$$

$$\times\delta_{ij}^\perp\hat{\alpha}_{j\mu}^{(m_1'm_1)}(\omega-\mathbf{k}\cdot\mathbf{v}_1)a_{\mathbf{k}\mu}. \quad (14)$$

Here, the intermediate and output frequencies are the following:

$$\omega_{12}=\omega-\omega_{m_1'm_1}+(\mathbf{k}_{12}-\mathbf{k})\mathbf{v}_1,$$

$$\omega_2 = \omega_{12} - \omega_{m_2' m_2} + (\mathbf{k}_2 - \mathbf{k}_{12}) \mathbf{v}_2, \tag{15}$$

where $\mathbf{v}_1$ and $\mathbf{v}_2$ are the velocities of the first and the second atoms, respectively. Then the intermediate and output wave vectors are given by

$$\mathbf{k}_{12} = \frac{\omega_{12}}{c} \frac{\mathbf{r}_2 - \mathbf{r}_1}{|\mathbf{r}_2 - \mathbf{r}_1|} \approx \frac{\omega}{c} \frac{\mathbf{r}_2 - \mathbf{r}_1}{|\mathbf{r}_2 - \mathbf{r}_1|},$$

$$\mathbf{k}_2 = \frac{\omega_2}{c} \frac{\mathbf{r} - \mathbf{r}_2}{|\mathbf{r} - \mathbf{r}_2|} \approx \frac{\omega}{c} \frac{\mathbf{r} - \mathbf{r}_2}{|\mathbf{r} - \mathbf{r}_2|}, \tag{16}$$

where the approximated expressions should be substituted in the Doppler terms. By $r_{12} = |\mathbf{r}_2 - \mathbf{r}_1|$, we denoted the relative distance between the atoms. The $\delta^{\perp}$ symbol is defined as follows:

$$\delta_{ij}^{\perp} = \delta_{ij} - \frac{k_{12i} k_{12j}}{k_{12}^2}, \tag{17}$$

and we use the set of Cartesian coordinates for tensor notation.

The full contribution of the fourth-order term is given by the sum

$$\hat{\mathbf{E}}_4^{(+)}(\mathbf{r}, t) = \hat{\mathbf{E}}_{4;1 \to 2}^{(+)}(\mathbf{r}, t) + \hat{\mathbf{E}}_{4;2 \to 1}^{(+)}(\mathbf{r}, t), \tag{18}$$

where the second term describes the scattering in the reverse sequence, i.e., on atom 2 first and on atom 1 second. It can be expressed by Eqs. (14)–(17) with replacement $1 \leftrightarrow 2$. In the case of backscattering, when $\mathbf{k}_1, \mathbf{k}_2 \sim -\mathbf{k}$ the output frequencies for both the sequences ω_1 and ω_2 have the same Doppler shift. But in a general situation, quantum mechanics allows that the initial states of the atoms $|m_1\rangle$ or $|m_2\rangle$ could be different for the direct and reciprocal paths contributing to Eq. (18), basically if atoms are in the superposed coherent states. Here, we restrict our discussion by assumption that the atoms occupy initially the certain states $|m_1\rangle$ and $|m_2\rangle$. Thus, the output frequency is equal for both the paths, i.e., $\omega' = \omega_2 = \omega_1$.

The double scattering cross section can be introduced similarly to Eq. (9)

$$d\sigma_{12} = \frac{\mathcal{V}}{2 \pi \hbar \omega'} \langle [\mathbf{e}'^* \hat{\mathbf{E}}_4^{(+)}(\mathbf{r}, t)]^{\dagger} \mathbf{e}'^* \hat{\mathbf{E}}_4^{(+)}(\mathbf{r}, t) \rangle r^2 d\Omega'$$

$$= d\sigma_{12}^{(L)} + d\sigma_{12}^{(I)}, \tag{19}$$

where the first term is the so-called ladder term describing the contribution of successive double scattering of the photon of the mode $\omega, \mathbf{k}, \mathbf{e}$ into the photon of the mode $\omega', \mathbf{k}', \mathbf{e}'$ along either the direct or reciprocal paths. This term can be expressed as follows:

$$d\sigma_{12}^{(L)} = \frac{\omega \omega'^3}{c^4} \frac{\omega_{12}^4}{c^4} \frac{1}{r_{12}^2} \left| \sum_{\nu \mu} \sum_{ij} e'^*_{\nu} \right.$$

$$\times \alpha_{\nu i}^{(m_2' m_2)}(\omega_{12} - \mathbf{k}_{12} \cdot \mathbf{v}_2)$$

$$\times \left. \delta_{ij}^{\perp} \alpha_{j\mu}^{(m_1' m_1)}(\omega - \mathbf{k} \cdot \mathbf{v}_1) e_{\mu} \right|^2 d\Omega' + \{1 \Leftrightarrow 2\}. \tag{20}$$

Here, we have written out the term which describes the scattering on atom 1 first and and on atom 2 second, i.e., along a direct path, and the unwritten term describes the scattering sequence in opposite order, i.e., along a reciprocal path. The reciprocal term can be reproduced by replacement of all the indices $1 \leftrightarrow 2$ in the direct term.

The cross section $d\sigma_{12}^{(I)}$ is responsible for the interference between direct and reciprocal paths and it is given by

$$d\sigma_{12}^{(I)} = \frac{\omega \omega'^3}{c^4} \frac{\omega_{12}^2}{c^2} \frac{\omega_{21}^2}{c^2} \frac{1}{r_{12}^2} \exp[i(\mathbf{k}' + \mathbf{k})(\mathbf{r}_1 - \mathbf{r}_2)$$

$$+ i(k_{12} - k_{21}) r_{12}] \sum_{\nu \mu} \sum_{\bar{\nu} \bar{\mu}} \sum_{ij} \sum_{\bar{i} \bar{j}} e'^*_{\nu}$$

$$\times \alpha_{\nu i}^{(m_2' m_2)}(\omega_{12} - \mathbf{k}_{12} \cdot \mathbf{v}_2) \delta_{ij}^{\perp} \alpha_{j\mu}^{(m_1' m_1)}(\omega - \mathbf{k} \cdot \mathbf{v}_1)$$

$$\times e_{\mu} e'_{\bar{\nu}} \alpha_{\nu \bar{i}}^{(m_1' m_1)*}(\omega_{21} - \mathbf{k}_{21} \cdot \mathbf{v}_1) \delta_{\bar{i} \bar{j}}^{\perp} \alpha_{\bar{j} \bar{\mu}}^{(m_2' m_2)*}$$

$$\times (\omega - \mathbf{k} \cdot \mathbf{v}_2) e^*_{\bar{\mu}} d\Omega' + \{1 \Leftrightarrow 2\}, \tag{21}$$

where the second unexpanded term is the complex conjugate of the expanded term. We assume here that the output photon has the propagation direction $\mathbf{k}'$ close to the direction $-\mathbf{k}$. That is, the most important situation when the effect of interference does not disappear after the averaging over the locations of atoms. But even so, the intermediate frequencies ω_{12} and ω_{21} as well as wave numbers k_{12} and k_{21} are distinguished because of the difference in the Doppler shifts, see Eq. (15).

Let us show, how the single- and double-scattering contributions manifest themselves in the scattering of one photon on a system of two atoms having random locations in space. The probability of backscattering can be written as follows:

$$dw \propto \left(1 - \frac{\sigma_2}{S} \theta_{21}\right)^2 d\sigma_1 + \left(1 - \frac{\sigma_1}{S} \theta_{12}\right)^2 d\sigma_2 + d\sigma_{12}. \tag{22}$$

Here σ_i with $i = 1, 2$ is the total cross section of the photon scattering on the ith atom, S is the spatial cross section of the light beam, $d\sigma_{12}$ is the cross section of double scattering in backward direction given by Eqs. (19)–(21). The symbol θ_{ij} is equal to $+1$ if atom i is located in front of atom j and is equal to zero otherwise. This expression has clear probabilistic nature and indicates the appearance of the well-known Bouguer-Lambert law. The power of two in the conditional

probabilities of Eq. (22) comes from the condition not to lose the photon on either incoming or on outgoing paths of backward scattering.

We conclude this part of our discussion by the following remark. The derived expressions for double scattering (19)–(21) are actually valid with less accuracy than the original Kramers-Heisenberg formula (9). There is an important physical restriction coming from the rotating wave approximation, which ignores any alternatives in the ordering of events of creation of the output or intermediate photons and annihilation of the input or intermediate photons. As is well-known, the first term in Eq. (9) is responsible for the order, when the output photon is created before the input photon was annihilated. That is not the case of expressions (19)–(21), which are based on a conception of step-by-step scattering along direct or reciprocal paths. Unfortunately, the first term in Eq. (9) is very small, and would be difficult to be observed or manifested in a multiple-scattering regime.

D. Multiple scattering

The results of the preceding section can be generalized to the situation of multiple scattering. In the multiple-scattering transformation of arbitrary order, considered on any chosen chain of atoms, the expressions (14) and (19)–(21) should be rewritten for the respective number of scatterers. But the important peculiarity of such a kind of generalization is that in triple and higher orders of scattering it is possible to include one atom in a scattering sequence several times. Such recurrent scattering has recently been observed by Wiersma, *et al.* [29].

To see this let us follow how formula (22) can be modified for the case of triple scattering in the system of three scatterers,

$$
\begin{aligned}
dw \propto & \left(1 - \frac{\sigma_2}{S}\theta_{21} - \frac{\sigma_3}{S}\theta_{31} + \frac{\sigma_2\sigma_3}{S^2}\theta_{21}\theta_{31}\right)^2 d\sigma_1 + \cdots + \left[\left(1 - \frac{\sigma_3}{S}\right)^2\theta_{31}\theta_{32} + \left(1 - \frac{\sigma_3}{S}\right)\left(1 - \frac{\sigma_3 r_{12}}{V_{12}}\right)(\theta_{13}\theta_{32} + \theta_{31}\theta_{23}) \right. \\
& \left. + \theta_{13}\theta_{23}\right] d\sigma_{12} + \cdots + \left[\left(1 - \frac{\sigma_3}{S}\right)^2\theta_{31}\theta_{32} + \left(1 - \frac{\sigma_3 r_{12}}{V_{12}}\right)^2\theta_{13}\theta_{32} + \left(1 - \frac{\sigma_3}{S}\right)^2\left(1 - \frac{\sigma_3 r_{12}}{V_{12}}\right)^2\theta_{31}\theta_{23} + \theta_{13}\theta_{23}\right] \\
& \times d\sigma_{121} + \cdots + d\sigma_{123},
\end{aligned}
\tag{23}
$$

where ellipses denote similar terms generated by all possible permutations and V_{12} is the macroscopic cylindrical volume located between atoms 1 and 2. In addition to the Bouguer-Lambert law, this expression has another example of conditional probabilities caused by macroscopic correction in lower orders in light scattering. Namely, if for any chosen chain of atoms there is a particular atom randomly located inside the chain, it can scatter the multiply scattered photon with some finite probability. This is the first macroscopic correction of the retarded or advanced Green's function of the photon propagating in a continuous medium.

In spite of the fact that the expansion (23) performs a straightforward generalization of Eq. (22), there are several important effects which appear, and which should be mentioned here. First, we see the indication of the Bouguer-Lambert law not only as a correction of the input probability for the photon scattered on one atom but also on a sequence of two atoms. Second, there is a contribution here of the triple scattering realized on the system of two atoms. This process suggests an initial indicator of strong localization, where light undergoes multiple scattering inside the chain. In the system of a large number of atoms this contribution is negligible because the photon can be scattered on any "new" atom with higher probability than on "previous" one. To increase the role of this process one needs to increase the mutual scattering amplitude among a selected number of atoms to enhance the internal multiscattering process. Third, we see that there is no macroscopic correction of the multiple-scattering cross section if the number of scattering events coincides with (or higher than) the number of scatterers. This number is equal to two in the example of Eq. (22) and three in the example of Eq. (23).

Let us follow now the modification arising when we apply our result up to the limit of a macroscopic number of atoms $N \to \infty$. In this situation, normally the order of the multiple scattering coincides with the optical thickness of the medium. As shown by calculations described in the following section, if the optical thickness has an order of 5 the order of multiple scattering contributing significantly to the backscattering is up to ten. This allows us to base our practical calculations on expressions (19)–(21) generalized and applied to an arbitrary number of atoms but taking into consideration only the chains containing different atoms. To make the macroscopic correction in the numerical procedure, we introduce additional Bouguer-Lambert-type attenuation for incoming and outgoing intensity and exponential attenuation in the retarded and advanced Green's function.

E. Effects of interference and polarization transformation in coherent backscattering

As we see from the basic expressions (19) and (20), if an atomic gas is sufficiently cold that Doppler shifts become negligible and $k_{12} \approx k_{21}$, the interference component in the backscattering cross section is not reduced after averaging over locations of atoms. In the optically dense medium this effect is preserved for any chain of any number of scatterers. It is known as weak localization of light and manifests itself

as an interferometric rise in intensity of scattered light in a narrow cone in the backscattering direction. In this paper, we are concerned with modeling coherent wave scattering in a sample of ultracold atoms confined to a magneto-optic trap. In the present case, the average atom temperature was measured to be less than 50 μK. As the Doppler shift is equal to the natural half-width for a temperature $T \sim 110$ mK, the approximation $k_{12} \approx k_{21}$ is valid in the present case. In addition, because of the experimental protocol, as described elsewhere [21], any optical lattice structure generated by the cooling lasers during the sample preparation becomes randomized before the coherent backscattering (CBS) measurements. Such effects, which are of considerable interest in their own right, are then ignored in the present treatment.

It is also well known that this coherent backscattering effect shows a pronounced and distinct dependence on the polarization state of both the incident and the detected light. It is then customary to define two orthogonal outgoing scattering channels for each of two-incident polarization states, the incident states being either linear or circular. In both cases, the electric-field vector of the scattered light is taken to be tangent to the detection plane, whose normal is then collinear with the exact backscattering direction. It is important to point out that the polarization analysis defined this way does not constitute a complete description of the scattered polarized light. In general, there are four Stokes parameters required to accomplish this, and with the two states defined above, along with the total intensity, only three are obtained in the customary method of analysis of coherent backscattering. In the exact backscattering direction, there is an axis of symmetry that makes the additional degree of freedom not necessary. However, for light scattered off the exact backwards direction, it is possible, for example, to observe a linear polarization degree of the scattered light when one of the incoming channels is in a pure helicity state. In the present paper, in order to make clear comparison with previous work, we examine only the standard coherent backscattering polarization channels.

The origin of the polarization dependence depends partly on the contribution of single-scattering events in relation to the multiple-scattering ones, and also on the nature of the scatterers themselves. For classical scatterers, in the absence of a Hanle effect, which corresponds to atomic scattering on a $^1S_0 \rightarrow {}^1P_1$ transition, the so-called linear in–linear parallel out (lin-par-lin) channel has a maximal enhancement factor of 2. This is a consequence of the reciprocity of the two-time reversed paths that correspond to the cone formation in the backscattering direction. However, for an atomic sample with degenerate ground and excited levels, it was recently shown that this full interference is partially lost due to the statistical nature of the Zeeman transitions made by each atom along a scattering chain. This was a surprising result, for at first sight it may seem natural to assume that only elastic Rayleigh scattering contributes to the coherent backscattering; one expects that this effect has a classical interference nature and the quantum nature only appears in a more complicated structure of the transition-matrix elements. However, the elastic Raman process also manifests itself in the interference part of the backscattering cross section. As
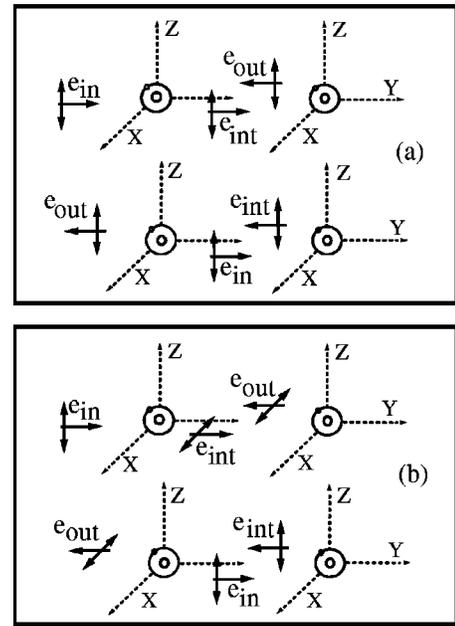

FIG. 1. Diagrams showing the direct and reciprocal paths for (a) Rayleigh-type and for (b) Raman-type coherent backscattering for two atoms linearly located along the propagation direction of the incident light.

pointed out originally by Labeyrie *et al.* [20], this leads to a strong suppression of the CBS enhancement factor.

It is instructive to demonstrate this by means of a specific example of a $|jm\rangle \rightarrow |j'm'\rangle$ optical transition (j and m are the atomic angular momentum and its projection, respectively) with $j = j' = 1$. In Fig. 1, the direct and reciprocal ways of interference in the Raman-type backscattering are shown for the special situation of only two atoms linearly located along the propagation direction of the incident light. The possibility of Raman-type interference can be understood from the transition diagrams shown in Fig. 2 in the basis

$$|x\rangle = \frac{1}{\sqrt{2}}(|1,-1\rangle - |1,+1\rangle),$$

$$|y\rangle = \frac{i}{\sqrt{2}}(|1,-1\rangle + |1,+1\rangle),$$

$$|z\rangle = |1,0\rangle, \tag{24}$$

which is more suitable for discussing the scattering of linearly polarized light, see Ref. [30]. The solid and dashed-dotted arrows in these diagrams indicate the transitions open for direct and reciprocal ways, respectively, which leads to the polarization transformation illustrated in Fig. 1.

However, we should point out that, even in this quite special example, it is not so obvious to predict how the situation would change if we introduced a small shift of the Zeeman sublevels or generated Zeeman coherence among these sublevels. The latter could be created in experiment by an optical pumping mechanism and additionally stimulated by low-
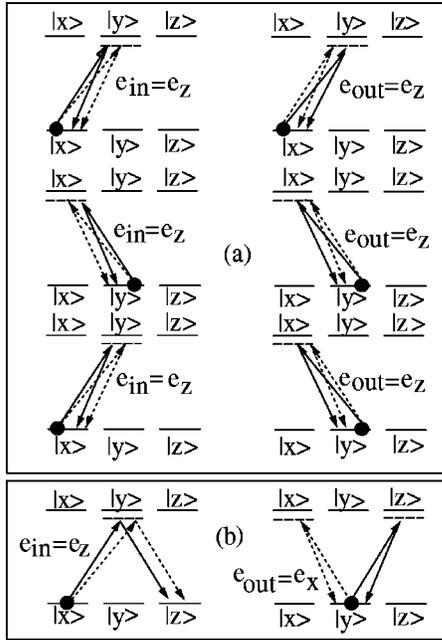
FIG. 2. Diagrams showing the transitions open for (a) Rayleigh-type and for (b) Raman-type coherent backscattering in the geometry of Fig. 1. In these diagrams the solid circles show the state designation of atoms and the solid and dashed arrows indicate the transitions open for direct and for reciprocal scattering paths, respectively.

frequency modulation of an external magnetic field. These points serve to illustrate that in the treatment of a realistic situation of multilevel atoms, the manifestation of atomic Zeeman coherence in the coherent Rayleigh-Raman back-scattering process can be the basis for many phenomena which may be important to achieve light localization in atomic vapors. One of the main objectives of this theoretical study is to make realistic predictions associated with specific situations as explored in the experimental parts of our research, see Ref. [21]. Further, once reliable *ab initio* results have been obtained, the techniques developed may be used to obtain predictions associated with more complex physical situations. Among those to be considered is the onset of strong-field effects; these will clearly become important as conditions for strong localization are approached. In addition, it would be interesting to consider those effects that may be initiated by coherences in the atomic subsystems, including Zeeman and hyperfine coherences.

III. NUMERICAL SIMULATION

In this section, we present an example of the numerical simulation of the backscattering process made for the nearly closed transition between ground $F_g = 3$ and excited $F_e = 4$ hyperfine sublevels of the D_2 line of ^{85}Rb, and for an ultra-cold atomic ensemble confined to a magneto-optic trap. In our modeling of the process, the external parameters were chosen to be typical of experimental conditions associated with atoms confined to a magneto-optic trap [19,21]. In addition, we have included the influence of nonresonant transi-

tions associated with the other electric dipole permitted $F_g \rightarrow F_e$ transitions on the coherent backscattering spatial and spectral profiles. The optically dense atomic cloud of rubidium atoms was approximated by a Gaussian-type distribution of scatterers with a resonant optical thickness, on the $F_g = 3 \rightarrow F_e = 4$ transition, varied from 2.5 to 5. If the spherically symmetric Gaussian-type density distribution is parameterized by

$$n(r) = n_0 \exp(-r^2/2r_0^2), \tag{25}$$

the optical thickness along any ray, crossing the cloud in its center, can be estimated as $\sqrt{2\pi}\sigma_0 n_0 r_0$, where σ_0 is the total cross section of resonance scattering, and the number of atoms in the cloud is $N = (2\pi)^{3/2} n_0 r_0^3$. For a closed transition, the resonance cross section σ_0 is given by

$$\sigma_0 \approx \frac{2(2F_e + 1)}{2F_g + 1} \frac{\pi}{k^2}. \tag{26}$$

Here, we use "approximately equal" sign to point out that this expression refers to a single-isolated resonance. As we will see, there will be an additional important contributions coming from light scattering from nonresonant hyperfine transitions. We point out that, in a more precise modeling of the real experimental conditions, the distribution (25) can be further generalized for an anisotropic cloud [22], where the dispersion r_0^2 should be chosen to be different for different directions.

The numerical procedure was based on a Monte Carlo method. For any macroscopic atomic ensemble containing N atoms, we randomly choose any chain of n scatterers with $n = 1,2,3,\ldots$. For such a chain, we calculate the ladder and interference contribution to the cross section following the method described in the preceding sections. In the basic expressions (20) and (21), we additionally introduced Bouguer-Lambert-type attenuation for incoming and outgoing waves as well as for the light propagation function between the atoms. For an ultracold atomic ensemble with typical temperatures less than 100 μK, we can neglect the Doppler shifts in the denominators of those expressions. After the averaging over many random choices of n scatterers the mean number has to be multiplied by $N!/n!(N-n)! \approx N^n/n!$, that is, by the number of all possible chains containing n atoms. The interferometric increase of the intensity of the backward-scattered light can be properly described in terms of a so-called enhancement factor (EF), which is defined as the ratio

$$X_{\text{EF}} = \frac{dw}{dw^{(L)}}, \tag{27}$$

where in the numerator we keep all the contributions of multiple scattering from both the ladder and interference terms, but in the denominator keep only the contributions of the ladder type. The enhancement factor indicates the interference rise of the intensity of the light scattered in the backward direction with respect to the incoherent background. Each of the probabilities can be constructed based on the
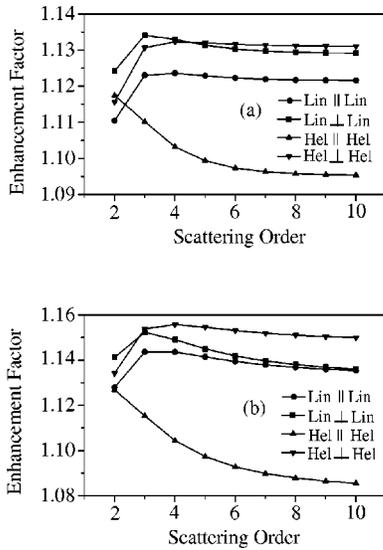
FIG. 3. The dependence of the enhancement factor, calculated for a $F_g=3 \rightarrow F_e=4$ hyperfine transition in ^{85}Rb, of the order of multiple scattering for a Gaussian-type atomic cloud with radius $r_0=1$ mm for two densities (a) $n_0=8 \times 10^9$ cm^{-3}, and (b) $n_0=16 \times 10^9$ cm^{-3}. Different curves relate to different polarizations of the scattered light with respect to either linear (lin) or circular (hel) input polarization.
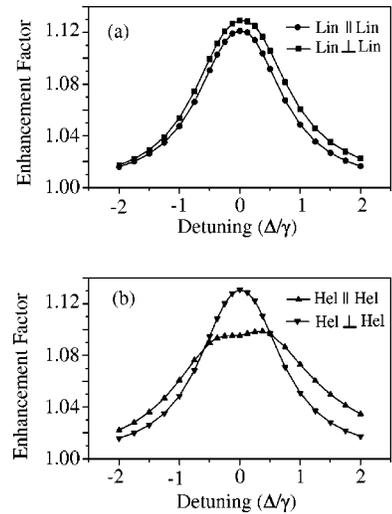

FIG. 4. The spectral behavior of the enhancement factor in the vicinity of the $F_g=3 \rightarrow F_e=4$ hyperfine transition in ^{85}Rb for (a) linear and (b) circular polarizations, calculated for a Gaussian-type atomic cloud with radius $r_0=1$ mm for density $n_0=8 \times 10^9$ cm^{-3}. The frequency detuning Δ is scaled in units of the natural linewidth γ

series introduced in Sec. D and extrapolated to a macroscopic number of atoms. But actually for a large number N, of the order of 10^9, it is sufficient to keep only the lower orders of multiple scattering and to consider the Bouguer-Lambert law in its macroscopic form. We also point out here that in our numerical analysis, we consider the realistic situation where there are typically only a few scattering events, conditions that pertain to the connected experimental study. It is important to realize that the present results, which may be compared quantitatively with an ultracold atomic sample of finite size, should only qualitatively be compared to the more common treatment of diffusive light transport in a semi-infinite medium.

IV. RESULTS AND DISCUSSION

In this section, we present details of our results for the spatial, spectral, and polarization dependence of near-backscattered light from a sample of ultracold Rb confined to a magneto-optical trap. We examine the influence of sample size and shape, and the dependence on atomic density. These show a wide range of phenomena that may be seen through the coherent backscattering effect in a resonant atomic medium.

First, we consider the convergence of the cone enhancement factor of the order of multiple scattering. These results are illustrated in Fig. 3, where we have plotted the dependence of the enhancement factor as a function of the order of multiple scattering taken into consideration. The enhancement factor was calculated for nominally resonant scattering on the $F_g=3 \rightarrow F_e=4$ hyperfine transition of the D_2 line of ^{85}Rb for different types of mutual polarization between inci-

dent and scattered waves. The calculations are presented here for two examples of atomic clouds having a Gaussian-type density distribution characterized by same radius $r_0=1$ mm but different peak densities in the center of the clouds of (a) $n_0=8 \times 10^9$ cm^{-3} and (b) $n_0=16 \times 10^9$ cm^{-3}. For these densities the optical thickness of the clouds is approximately varied from 2.5 to 5. As the basic scaling parameter of the present treatment is $n_0(\lambda/2\pi)^3$, which is $\sim 10^{-4}$ and quite far from the regime of dependent scattering, the present numerical results should apply to the typical situation of ultracold atoms in a not-too-dense magneto-optic trap. Then, as follows from these graphs when the scattering order becomes higher than ten all the curves appear to nearly approach a saturation limit. However, there is a small but not negligible difference between the curves corresponding to any type of mutual polarization but different optical thicknesses. Such a difference indicates that the polarization dependence of the process is quite sensitive to the ratio of the length of the photon free path in the medium to the size of the cloud.

The selective analysis of the different orders of multiple scattering can be made in experiment via the observation of the spectral dependence of the enhancement factor in the vicinity of the resonance line. Indeed, higher orders of multiple scattering give a contribution near the central point of this line, but the lower orders become more important in its wing. In Figs. 4 and 5, we show the spectral profile of the enhancement factor for different types of mutual polarization between incident and scattered light as function of the frequency detuning Δ in units of natural linewidth γ. As in Fig. 3, the calculations were made for two examples of atomic clouds with Gaussian-type density distribution characterized by the same radius of the clouds $r_0=1$ mm but different central densities of $n_0=8 \times 10^9$ cm^{-3} (Fig. 4) and $n_0=16 \times 10^9$ cm^{-3} (Fig. 5). Comparing the spectral curves
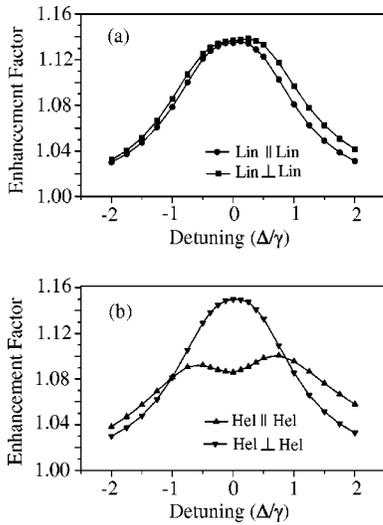
FIG. 5. The spectral behavior of the enhancement factor, for the $F_g=3\rightarrow F_e=4$ hyperfine transition in ^{85}Rb for (a) linear and (b) circular polarizations, calculated for a Gaussian-type atomic cloud with radius $r_0=1$ mm for density $n_0=16\times10^9$ cm^{-3}. The frequency detuning Δ is scaled in units of the natural linewidth γ.

plotted in Figs. 4 and 5 with the corresponding dependencies plotted in Fig. 3 one sees that there is a certain correlation between the spectral behavior of the enhancement factor and its dependence on the order of multiple scattering.

The most important feature of the dependences shown in Figs. 4 and 5 is in the asymmetric shape of the spectral profiles, when the detection scheme is the Raman type, with orthogonal linear polarizations or with preserving the helicities of incoming and outgoing waves. Helicities are defined with respect to the frame associated with the running waves. Thus, for the helicity preserving channel in the backward scattering direction as defined in the laboratory frame, there is an opposite rotation for the polarization vectors of the incoming and outgoing waves. With that definition, the asymmetric shape of the spectral profile is more clearly seen in the case of circular polarization. This indicates the non-trivial spectral behavior of the Raman-type interference terms and the Raman-type ladder terms near the resonance. Let us point out that the asymmetric shape of the spectral profiles shown in Figs. 4 and 5 does not arise directly from the variation of the scattering order with optical depth, but instead comes from interference of the scattering amplitudes of near resonant and other nonresonant hyperfine transitions within the entire hyperfine multiplet, which were taken into consideration in our calculation. This was unambiguously established by formally keeping only the $F_g=3\rightarrow F_e=4$ transition, in which case a symmetric spectral profile results. In other words, the asymmetric spectral behavior of the enhancement factor near the resonance is an indication that for light scattering in an optically dense medium, all the near-resonant scattering channels become important. We also mention here that for an atomic ensemble, where on an average the atoms are separated by a distance of the order of a few optical wavelengths, the calculated spectral profiles should show directly the multiple-scattering behavior in a
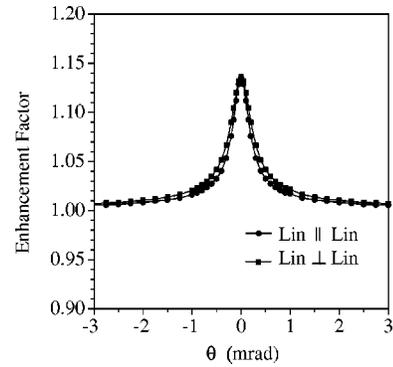
spectral domain narrow compared to the natural width. In particular, we might expect that in the wings of the spectral line, of the order of a few natural widths, the long-range dipole-dipole interaction will both modify the atomic pair distributions and lead to optical modification of the light transport in the medium. In fact, when atom pairs become located on the average inside an optical wavelength, the basic approximation of the present work, where light transport is a sequence of independent scattering events will break down. Experimental study of the detuning dependence of the cone enhancement, including effects of density and off-resonant transitions is currently underway in our laboratory.

Next, consider the cone spatial profile for four polarization channels and for a symmetric MOT of size parameter r_0. In Figs. 6 and 7, we show the cone profile when ten orders of multiple scattering were taken into account in the calculations. Both the graphs show the dependence of the enhancement factor on the backscattering angle θ, which is the offset from the backward direction, for the cloud with $r_0=1$ mm and $n_0=16\times10^9$ cm^{-3}. In Fig. 6, the enhance-
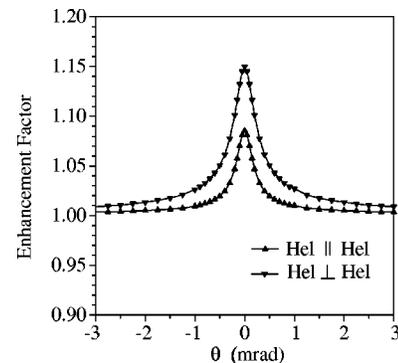

FIG. 6. The dependence of the enhancement factor on the backscattering angle θ for the $F_g=3\rightarrow F_e=4$ hyperfine transition in^{85}Rb and for a Gaussian-type atomic cloud with radius $r_0=1$ mm and for density $n_0=16\times10^9$ cm^{-3}. The two curves relate to linear parallel and linear orthogonal mutual polarizations between the incident and scattered light.

FIG. 7. The dependence of the enhancement factor on the backscattering angle θ for the $F_g=3\rightarrow F_e=4$ hyperfine transition in ^{85}Rb and for a Gaussian-type atomic cloud with radius $r_0=1$ mm and for density $n_0=16\times10^9$ cm^{-3}. The two curves relate to the identical and orthogonal helicities of the incident and scattered light.
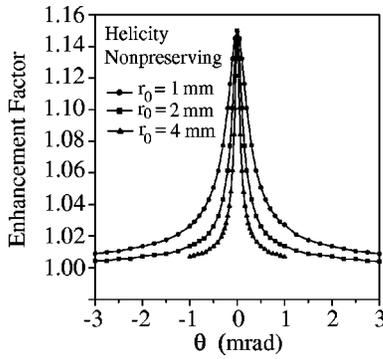
FIG. 8. Sample size dependence of the spatial profile of the coherent backscattering cone in the helicity nonpreserving channel.

FIG. 9. Dependence on the inverse sample size of the full width at half maxiumum of the coherent backscattering cone for four polarization channels. The optical depth is fixed at five for these calculations.

ment factor is plotted for linear polarized incident light and for linear parallel (lin∥lin) and linear perpendicular (lin⊥lin) polarization of scattered light. For this particular graph, the angle θ describes scanning in a horizontal (perpendicular to the polarization of incident light) plane. In Fig. 7, the enhancement factor is plotted for circularly polarized incident light and for the identical (hel∥hel) and orthogonal (hel⊥hel) helicities of the scattered light. The important feature of the graphs plotted in Fig. 6 is that for an optically dense medium, where multiple scattering dominates, there is only a slight difference in the backscattering response for Rayleigh (lin∥lin) and Raman-(lin⊥lin) type scattering. But that is not the case for the circular polarized light with the cone profile plotted in Fig. 7, where Rayleigh-type backscattering with hel⊥hel manifests itself as more effective process.

We have also investigated the dependence of the spatial profile of the CBS cone on the size of the atomic sample. For the Gaussian density distribution defined previously, we have varied the effective radius r_0 in the range $(1-4)$ mm, while keeping the optical depth of the sample constant at a value of about 5. Recall that the optical depth is defined for a Gaussian MOT as $\sqrt{2\pi}\sigma_0 n_0 r_0$. Note that this corresponds to decreasing the atomic density as the radius increases. CBS cones for helicity nonpreserving polarization channel is shown in Fig. 8. In the figure, it is seen that the enhancement factor does not measurably change with sample size. With reference to Figs. 3, 6, and 7, this is not surprising, as the enhancement is nearly asymptotic for the higher-order scattering, which dominates the very small angle enhancement. However, it is important to note that the wings of the cones are significantly elevated, illustrating that the lower orders of scattering become more important in angular directions off exact backscattering. On the other hand, the full width at half maximum of the enhancement relative to the incoherent background is seen to *increase* significantly with *decreasing* sample size. The origin of this effect illustrates one of the fundamental differences between the more traditional scattering off a nearly semi-infinite medium, where there may be scattering paths of any length, and scattering off a finite medium, where the higher-order scattering contains paths that fill the volume of the medium. In this case, which applies to our results, the average path is comparable to the size of the
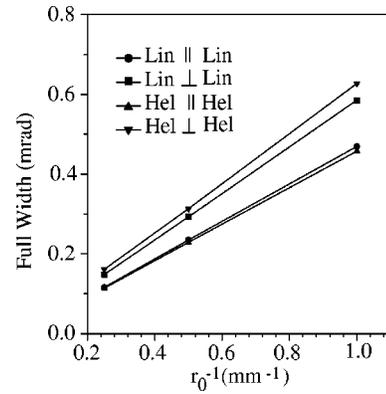
sample, and so the width of the cone $\Delta\theta\sim1/kL$, where L in this case is a characteristic length scale defining the size of the medium. In our case, that is, the parameter r_0, and so we expect that the cone width will generally decrease as L increases. This behavior is seen in Fig. 8, and is illustrated in Fig. 9 for the four polarization channels considered. Note that in the size and optical depth range considered here, the full width at half maximum of the enhancement depends linearly on the reciprocal of the characteristic size parameter. However, there is only a weak dependence on the cone profile for samples of a fixed size, but not too different density.

Next, we consider comparison of the theoretical results developed here with recent experiments [21]. In order to make this comparison, it is necessary to take into account as nearly as possible the spatial asymmetry of real ultracold samples confined in a magneto-optic trap. Because of the different force constants associated with the magnetic-field gradient in a typical MOT, the atomic samples are not typically Gaussian, although under some circumstances they may be quite close to that shape. For the atomic Rb MOT used in the experiments associated with this study, the MOT is "cigar shaped" and has size parameters r_0 of about 0.55 mm for the width and 0.69 mm for the height. As described elsewhere [21], these values are obtained by fluorescence imaging of the MOT excited by light detuned several γ from resonance, where γ is the natural line width of the resonance transition. Although a detailed theoretical and experimental examination of the influence of the MOT shape and inhomogeneous atom distributions (25) will be developed in a later report, we present a comparison in Fig. 10 of experimental and theoretical results for an asymmetric MOT having size parameters corresponding to the conditions of the experiment. For this comparison we have selected the lin-par-lin polarization channel, which has the experimental advantage of a greatly suppressed environmental background. It is seen in the figure that the agreement is extraordinarily good in terms of the overall profile shape and enhancement. The slight differences in widths for the two cases is likely due to a slight overestimate of the size of the MOT by the fluorescence imaging technique. In any case, scaling from the sym-
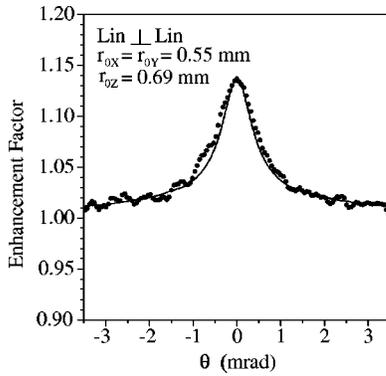
FIG. 10. Comparison between experimental and theoretical results for the spatial profile of the coherent backscattering cone in the lin-per-lin polarization channel. The calculations correspond closely to the experimental conditions where the optical depth is ~ 5, and the sample is cigar shaped having $1/e^2$ diameters of 2.20 mm and 2.76 mm.

FIG. 12. Asymmetry of the spatial profile of the coherent backscattering cone in the lin-par-lin polarization channel. Scanning is either perpendicular to or parallel to the electric-field direction of the incident and scattered light. The calculations correspond closely to the experimental conditions, where the optical depth is ~ 5, and the sample is cigar shaped having $1/e^2$ diameters of 2.20 mm and 2.76 mm.

metric MOT case, we estimate that the difference is well within the experimental uncertainty in the size parameters. We point out here that there also is a weaker dependence on the width due to the optical thickness of the MOT. In this case, we allow the MOT size to remain fixed and at the values set by the experiment, and vary the optical depth. The result for two different number densities (optical depths at fixed size parameters) is shown in Fig. 11. It is seen there that the small differences between experiment and theory could also result from an underestimate in the measurement of the optical depth.

Finally, we consider the angular dependence of the shape of the cone about the direction of the incident wave vector. These results are illustrated for the lin-par-lin polarization channel in Fig. 12, which shows the cone profile for angular scanning either perpendicular to or parallel to the direction of the electric field of the incident light. There it is seen that for scanning along the direction of the incident electric field the cone is nearly two times wider than it is when scanning perpendicular to the direction of the incident field. This ef-

fect has previously been observed in experiments by Labeyrie *et al.* [20], and by Kulatunga *et al.* [21]. It is due to the strong influence of lower-order scattering in these experiments, and the angular dependence of the single-scattering differential cross-section. As the angular dependence even for an $F_g = 3 \rightarrow F_e = 4$ transition resembles strongly that of a classical dipole, the variations in the angular distribution for scattering in the parallel direction show nearly stationary variations of the phase in this direction. This result also shows that interpretation of the width and shape of the coherent backscattering spatial profile requires consideration of the tensorial nature of the scattering as well as the geometrical features of the sample.

V. SUMMARY AND CONCLUSIONS

In this paper, we have described in detail theoretical treatment of coherent backscattering of light from an ultracold atomic gas of ^{85}Rb. We have developed the basic theoretical expressions and numerically simulated the spectral and spatial shape of the coherently backscattered radiation for four standard polarization channels. Application was to ultracold Gaussian atomic distributions in a range of sizes and optical depths characteristic of atomic samples confined in magneto-optic traps. In a comprehensive study of the dependence of the spatial and spectral profile on the sample parameters and polarization, we have found that the enhancement and width of the coherent backscattering line shape is in excellent quantitative agreement with experimental results. In addition, although the enhancement does not strongly depend on the atomic sample size, for fixed optical depth the width of the backscattering cone decreases as the sample size increases. Finally, we predict a remarkable effect in which far-off-resonant hyperfine transitions have an exceptionally strong influence on the spectral dependence of the enhancement. This effect, although present in all polarization channels, dominates the Raman-type helicity preserving channel.
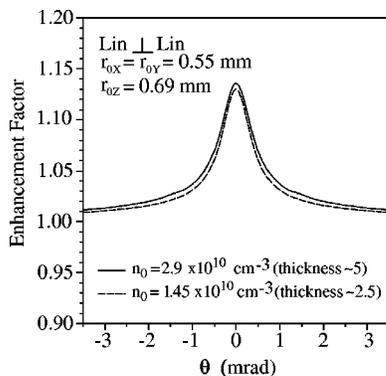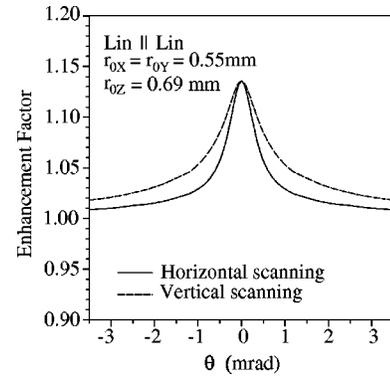

FIG. 11. Sensitivity to density of the spatial profile of the coherent backscattering cone in the lin-per-lin polarization channel. The calculations correspond closely to the experimental conditions of a cigar shaped sample having $1/e^2$ diameters of 2.20 mm and 2.76 mm, but for two different optical thicknesses ~ 2.5 and ~ 5.

[1] G. Placzek, *Rayleigh-Streuung und Raman Effekt, Handbuch der Radiologie* (Akademische Verlagsgesellschaft, Leipzig, 1934).

[2] M.D. Lukin, S.F. Yelin, and M. Fleischhauer, Phys. Rev. Lett. **84**, 4232 (2000).

[3] D.F. Phillips, A. Fleischhauer, A. Mair, R.L. Walsworth, and M.D. Lukin, Phys. Rev. Lett. **86**, 783 (2001).

[4] B. Julsgaard, A. Kozhekin, and E.S. Polzik, Nature (London) **413**, 400 (2001).

[5] D.S. Wiersma, P. Bartolini, Ad Lagendijk, and R. Righini, Nature (London) **390**, 671 (1997); A.A. Chabanov, M. Stoytchev, and A.Z. Genack, *ibid.* **404**, 850 (2000).

[6] Ping Sheng, *Wave Scattering, Localization, and Mesoscopic Phenomena* (Academic Press, San Diego, 1995).

[7] Ad Lagendijk and B.A. van Tiggelen, Phys. Rep. **270**, 143 (1996).

[8] J. Ishimaru and Y. Kuga, J. Opt. Soc. Am. A **1**, 813 (1984); M.P. VanAlbada and A. Lagendijk, Phys. Rev. Lett. **55**, 2692 (1985); P.E. Wolf and G. Maret, *ibid.* **55**, 2696 (1985).

[9] A.A. Golubentsev, Sov. Phys. JETP **59**, 26 (1984).

[10] E. Akkermans, P.E. Wolf, and R. Maynard, Phys. Rev. Lett. **56**, 1471 (1986).

[11] H. Cao, J.Y. Xu, D.Z. Zhang, S.-H. Chang, S.T. Ho, E.W. Seelig, X. Liu, and R.P.H. Chang, Phys. Rev. Lett. **84**, 5584 (2000).

[12] D.S. Wiersma, M.P. van Albada, and A. Lagendijk, Phys. Rev. Lett. **75**, 1739 (1995).

[13] M.B. van der Mark, M.P. van Albada, and Ad Lagendijk, Phys. Rev. B **37**, 3575 (1988).

[14] Ad Lagendijk, in *Current Trends in Optics*, edited by J. C. Dainty (Academic Press, London, 1994).

[15] P.W. Anderson, Phys. Rev. **109**, 1492 (1958).

[16] Martin Janssen, *Fluctuations and Localization in Mesoscopic Electron Systems* (World Scientific, Singapore, 2001).

[17] A.A. Chabanov and A.Z. Genack, Phys. Rev. Lett. **87**, 153901 (2001).

[18] A.A. Chabanov, M. Stoytchev, and A.Z. Genack, Nature (London) **404**, 850 (2000).

[19] Harold J. Metcalf and Peter van der Straten, *Laser Cooling and Trapping* (Springer, New York, 1999).

[20] G. Labeyrie, F. deTomasi, J.-C. Bernard, C.A. Muller, C. Miniatura, and R. Kaiser, Phys. Rev. Lett. **83**, 5266 (1999); G. Labeyrie, C.A. Muller, D.S. Wiersma, Ch. Miniatura, and R. Kaiser, J. Opt. B: Quantum Semiclassical Opt. **2**, 672 (2000).

[21] P. Kulatunga, C.I. Sukenik, S. Balik, M.D. Havey, D.V. Kupriyanov, and I.M. Sokolov (unpublished).

[22] Robin Kaiser (private communication).

[23] T. Jonckheere, C. Muller, R. Kaiser, Ch. Miniatura, and D. Delande, Phys. Rev. Lett. **85**, 4269 (2000).

[24] C.A. Muller, T. Jonckheere, C. Miniatura, and D. Delande, Phys. Rev. A **64**, 053804 (2001).

[25] R. Lenke and G. Maret, Eur. Phys. J. B **17**, 171 (2000).

[26] B.A. van Tiggelen, in *Coherent Matter Waves*, edited by R. Kaiser, C. Westbrook, and F. David (EDP Sciences, Les Ulis, 2001).

[27] Th.M. Nieuwenhuizen, A.L. Burin, Yu. Kagan, and G.V. Shlyapnikov, Phys. Lett. **184A**, 360 (1994).

[28] V.B. Berestetskii, E.M. Lifshitz, and L.P. Pitaevxskii, *Quantum Electrodynamics, Course of Theoretical Physics, IV* (Pergamon Press, Oxford, England, 1982).

[29] D.S. Wiersma, M.P. van Albada, B.A. van Tiggelen, and Ad Lagendijk, Phys. Rev. Lett. **74**, 4193 (1995).

[30] D.A. Varshalovich, A.N. Maskalev, and V.K. Khersonskii, *Quantum Theory of Angular Momentum* (World Scientific, Singapore, 1988).